J|A|C|S
ARTICLES
Published on Web 05/16/2006

Shape-Controlled Synthesis of Ternary Chalcogenide $ZnIn_2S_4$ and $CuIn(S,Se)_2$ Nano-/Microstructures via Facile Solution Route

Xinglong Gou, Fangyi Cheng, Yunhui Shi, Li Zhang, Shengjie Peng, Jun Chen,* and Panwen Shen

Contribution from the Institute of New Energy Material Chemistry, College of Chemistry, Nankai University, Tianjin 300071, P. R. China

Received November 29, 2005; E-mail: chenabc@nankai.edu.cn

Abstract: We demonstrated in this paper the shape-controlled synthesis of $ZnIn_2S_4$, $CuInS_2$, and $CuInSe_2$ nano- and microstructures through a facile solution-based route. One-dimensional $ZnIn_2S_4$ nanotubes and nanoribbons were synthesized by a solvothermal method with pyridine as the solvent, while $ZnIn_2S_4$ solid or hollow microspheres were hydrothermally prepared in the presence of a surfactant such as cetyltrimethylammonium bromide (CTAB) or poly(ethylene glycol) (PEG). The mechanisms related to the phase formation and morphology control of $ZnIn_2S_4$ are proposed and discussed. The UV−vis absorption spectra show that the as-prepared nano- and micromaterials have strong absorption in a wide range from UV to visible light and that their band gaps are somewhat relevant to the size and morphology. The photoluminescence measurements of the $ZnIn_2S_4$ microspheres at room temperature reveal intense excitation at ~575 nm and red emission at ~784 nm. Furthermore, $CuInS_2$ and $CuInSe_2$ with different morphologies such as spheres, platelets, rods, and fishbonelike shapes were also obtained by similar hydrothermal and solvothermal synthesis.

1. Introduction

Controlling the shape, size, and structure of inorganic nanomaterials is of fundamental importance because of the strong correlation between these parameters and physical/chemical properties.[1] Among various strategies for controlled synthesis, the "soft chemistry" route, which is based on a solution process, is an effective method for the chemical synthesis of nanostructural materials with well-controlled shapes, sizes, and structures.[2] For example, a variety of chalcogenide compounds with desired shape, morphology, and crystal phase were achieved by applying solution chemistry approaches.[3,4] Recently, semiconducting materials of ternary chalcogenide compounds AB_mC_n (A = Cu, Ag, Zn, Cd, etc.; B = Al, Ga, In; C= S, Se, Te) have gained much attention because they display tunable electronic and optical properties.[5−7] As typical ternary chalcogenide materials, $CuInSe_2$ and $CuInS_2$ have been intensively studied for applications in solar cells.[8,9] While $ZnIn_2S_4$ is also of interest because it has been demonstrated to have potential applications in different fields such as charge storage,[10] thermoelectricity,[11] electrochemical recording,[12] and photocatalysts.[13] However, the development of chemical methods suitable for the synthesis of $ZnIn_2S_4$ with controlled shape and size still remains a major challenge. In particular, to the best of our knowledge, there has been no report on the synthesis and optical property study of $ZnIn_2S_4$ one-dimensional (1-D) nanostructures.

Since the shape, size, and dimensionality of semiconductors are vital parameters for their properties,[14] developing a facile method to synthesize ternary chalcogenide materials with various morphologies is of interest and importance for their further

(1) (a) Hupp, J. T.; Poeppelmeier, K. R. *Science* **2005**, *309*, 2008. (b) Law, M.; Goldberger J.; Yang P. D. *Annu. Rev. Mater. Res.* **2004**, *34*, 83. (c) Sun, Y.; Xia, Y. *Science* **2002**, *298*, 2176.
(2) (a) Song, H.; Rioux, R. M.; Hoefelmeyer, J. D.; Komor, R.; Niesz, K.; Grass, M.; Yang, P. D.; Somorjia, G. A. *J. Am. Chem. Soc.* **2006**, *128*, 3027. (b) Wang, X.; Zhuang, J.; Peng, Q.; Li, Y. *Nature* **2005**, *437*, 121. (c) Cushing, B. L.; Kolesnichenko, V. L.; O'Connor, C. J. *Chem. Rev.* **2004**, *104*, 3893.
(3) (a) Gur, I.; Fromer, N. A.; Geier, M. L.; Alivisatos, A. P. *Science* **2005**, *310*, 462. (b) Zhang, L.; Yu, J. C.; Mo, M.; Wu, L.; Li, Q.; Kwong, K. W. *J. Am. Chem. Soc.* **2004**, *126*, 8116.
(4) (a) Duxin, N.; Liu, F.; Vali, H.; Eisenberg, A. *J. Am. Chem. Soc.* **2005**, *127*, 10063. (b) Peng, Q.; Dong, Y.; Li, Y. *Angew. Chem., Int. Ed.* **2003**, *42*, 3027. (c) Peng, Z. A.; Peng, X. *J. Am. Chem. Soc.* **2002**, *124*, 3343.
(5) (a) Castro, S. L.; Bailey, S. G.; Raffaelle, R. P.; Banger, K. K.; Hepp, A. F. *J. Phys. Chem. B* **2004**, *108*, 12429. (b) Banger, K. K.; Jin, M. H. C.; Harris, J. D.; Fanwick, P. E.; Hepp, A. F. *Inorg. Chem.* **2003**, *42*, 7713.
(6) (a) Tran, D. T. T.; Beltran, L. M. C.; Kowalchuk, C. M.; Trefiak, N. R.; Taylor, N. J.; Corrigan, J. F. *Inorg. Chem.* **2002**, *41*, 5693. (b) Jiang, Y.; Wu, Y.; Mo, X.; Yu, W.; Xie, Y.; Qian, Y. *Inorg. Chem.* **2000**, *39*, 2964.
(7) (a) Zheng, R. B.; Yang, X. G.; Hu, H. M.; Qian, Y. T. *Mater. Res. Bull.* **2004**, *39*, 933. (b) Castro, S. L.; Bailey, S. G.; Raffaelle, R. P.; Banger, K. K.; Hepp, A. F. *Chem. Mater.* **2003**, *15*, 3142. (c) Lu, Q.; Hu, J.; Tang, K.; Qian, Y.; Zhou, G.; Liu, X. *Inorg. Chem.* **2000**, *39*, 1606.
(8) (a) Nanu, M.; Schoonman, J.; Goossens, A. *Nano Lett.* **2005**, *5*, 1716. (b) Nanu, M.; Schoonman, J.; Goossens, A. *Adv. Funct. Mater.* **2005**, *15*, 95. (c) Arici, E.; Sariciftci, N. S.; Meissner, D. *Adv. Funct. Mater.* **2003**, *15*, 165.
(9) (a) Hermann, J.; Benfarah, M.; Bruneau, S.; Axente, E.; Coustillier, G.; Itina, T.; Guillemoles, J. F.; Alloncle, P. *J. Phys. D: Appl. Phys.* **2006**, *39*, 453. (b) Klenk, R.; Klaer, J.; Scheer, R.; Lux-Steiner, M. C.; Luck, I.; Meyer, N.; Rühle, U. *Thin Solid Films* **2005,** *480*−*481*, 509. (c) Jayadevan, K. P.; Tseng, T. Y. *J. Nanosci. Nanotechnol.* **2005**, *5*, 1768.
(10) Romeo, N.; Dallaturca, A.; Braglia, R.; Sberveglieri, G. *Appl. Phys. Lett.* **1973**, *22*, 21.
(11) Seo, W. S.; Otsuka, R.; Okuno, H.; Ohta, M.; Koumoto, K. *J. Mater. Res.* **1999**, *14*, 4176.
(12) Kazan, B.; Stig, B. M. U.S. Patent 4,826,732, May 2, 1989.
(13) Lei, Z. B.; You, W. S.; Liu, M. Y.; Zhou, G. H.; Takata, T.; Hara, M.; Domen, K.; Li, C. *Chem. Commun.* **2003**, 2142.
(14) Burda, C.; Chen, X.; Narayanan, R.; El-Sayed, M. A. *Chem. Rev.* **2005**, *105*, 1025.

10.1021/ja0580845 CCC: $33.50

applications. Here we report on a shape-controlled synthesis of $ZnIn_2S_4$ through a simple solution chemistry route. Using a combination of a solvothermal/hydrothermal method and surfactant template technique, we have obtained $ZnIn_2S_4$ materials with distinct and well-defined morphologies, including nanotubes, nanoribbons, nanowires, and microspheres, by controlling the reaction conditions. This type of one-pot synthesis route is carried out under mild reaction conditions, and no catalyst is required. Thus, the present solution-based route for the preparation of $ZnIn_2S_4$ nano- and microstructures is simple and controllable, which can be also extended to the synthesis of $CuInS_2$ and $CuInSe_2$ with different surface morphologies such as spheres, platelets, rods, and fishbonelike shapes. In addition, the UV−vis absorption measurements show that the as-prepared $ZnIn_2S_4$ materials have strong absorptions in a wide range from UV to visible light and that their band gaps are somewhat relevant to the size/morphology. The photoluminescence spectra of $ZnIn_2S_4$ microspheres at room temperature reveal intense excitation at ∼575 nm and red emission at ∼784 nm.

2. Experimental Section

Synthesis. $ZnIn_2S_4$ nanotubes and nanoribbons were synthesized via a solvothermal route from the reaction of zinc sulfate, indium chloride, and thioacetamide (TAA), with pyridine (Py) as the solvent. $ZnIn_2S_4$ microspheres were prepared by a hydrothermal synthetic method in the presence of a surfactant, either a cationic surfactant cetyltrimethylammonium bromide (CTAB) or a nonionic surfactant poly(ethylene glycol) (PEG). The chemical reactions involved in the solvothermal and hydrothermal synthesis can be briefly described as

$$ZnSO_4 + InCl_3 + CH_3CSNH_2 \xrightarrow[\geq 180^oC]{Py} ZnIn_2S_4\ (\text{nanotubes}) \quad (1)$$

$$\xrightarrow[\leq 160^oC]{} ZnIn_2S_4\ (\text{nanoribbons})$$

$$ZnSO_4 + InCl_3 + CH_3CSNH_2 \xrightarrow[\text{CTAB or PEG}]{H_2O} ZnIn_2S_4\ (\text{microspheres}) \quad (2)$$

All of the chemical reagents were of analytical grade and used without further purification. In a typical synthesis of $ZnIn_2S_4$ nanotubes, $ZnSO_4{\cdot}7H_2O$ (0.25 mmol), $InCl_3{\cdot}4H_2O$ (0.5 mmol), and TAA (2 mmol) were loaded into a 25 mL Teflon-lined autoclave, which was then filled with 12 mL of pyridine. After 1 h of magnetic stirring, the autoclave was sealed and maintained at 180 °C for 16 h and then allowed to cool to room temperature naturally. The yellow product was collected by centrifugation, washed several times with absolute ethanol and distilled water, and finally dried under a vacuum at 60 °C for 4 h. Similarily, $ZnIn_2S_4$ nanoribbons were prepared under the same conditions, except that the reaction temperature was maintained in the range 120−160 °C. Other reaction parameters that are influential to solvothermal synthesis such as reaction temperature, heating time, and solvent were also investigated in order to better understand the reaction mechanisms.

A typical synthesis of $ZnIn_2S_4$ microspheres follows the procedure as described below. First, $ZnSO_4{\cdot}7H_2O$ (0.2940 g) and $InCl_3{\cdot}4H_2O$ (0.6242 g) were dissolved in a beaker with deionized water (20.0 mL). Second, either CTAB (0.2606 g) or PEG-6000 (0.4418 g) was added into the solution under magnetic stirring until it was dissolved completely. Thioacetamide (TAA, 0.6048 g) was added in with continuous stirring, and the mixture was transferred into a Teflon-lined stainless steel autoclave of 50 mL capacity. Finally, the autoclave was sealed and maintained at 160 °C for 16 h and then cooled to room temperature naturally. The collecting, washing, and drying of the product followed the same treatment procedures as presented above. The $ZnIn_2S_4$ nanowires were obtained by ultrasonic dispersion of the PEG 6000-assisted sample for 60 min.

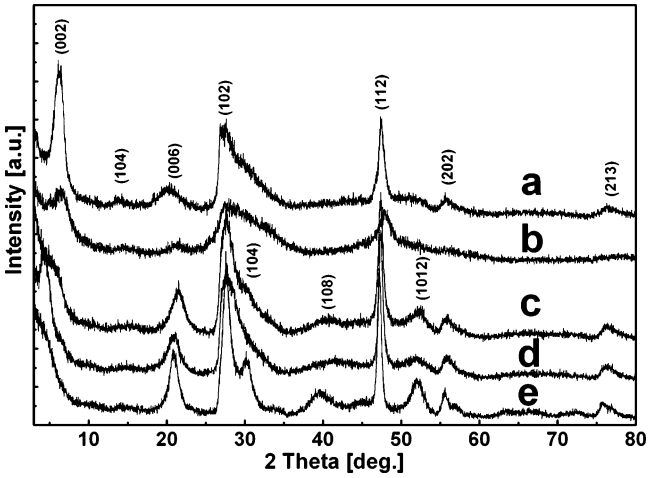

Figure 1. XRD patterns of the $ZnIn_2S_4$ products: (a) nanotubes and (b) nanoribbons prepared by solvothermal methods, (c) nanoflakes prepared by a hydrothermal method without any surfactant, (d) microspheres prepared by a hydrothermal method with CTAB, (e) microspheres prepared by a hydrothermal method with PEG-6000.

Characterization Techniques. Powder X-ray diffraction (XRD) patterns of the prepared samples were recorded on a Japan Rigaku D/max-2500 X-ray diffractometer with graphite monochromatized Cu Kα (λ = 1.5405 Å) radiation at a scanning speed of 4°/min in 2θ ranging from 3° to 80°. Inductively coupled plasma (ICP) emission spectroscopy measurement was performed on a Hitachi P-5200 analysis system. Transmission electron microscopy (TEM) and high-resolution TEM (HRTEM) analyses were carried out under a Philips Tecnai F20 microscope operating at an accelerating voltage of 200 kV. Scanning electron microscopy (SEM) images were taken using a Philips XL-30 and a JEOL JSM-6700F microscope. UV−visible diffuse reflectance spectra were recorded at room temperature on a JASCO V-550/V-570 UV−vis spectrophotometer fitted with an integrating sphere diffuse reflectance accessory. A photoluminescence (PL) measurement was taken at room temperature with a Varian Cary Eclipse fluorescence spectrophotometer.

3. Results

$ZnIn_2S_4$ was successfully synthesized through a simple one-pot approach employing solvothermal/hydrothermal reaction of zinc sulfate ($ZnSO_4$), indium chloride ($InCl_3$), and thioacetamide (TAA). The influence of synthesis conditions on the morphology of the product was studied by altering solvents, surfactants, and other parameters such as reaction temperature and heating time.

Structural Determination. The elemental contents of Zn, In, and S of all the samples were analyzed by ICP, and the atomic ratios were close to the stoichiometric composition. The phase and crystallographic structure of the products were determined by powder X-ray diffraction (XRD). Figure 1a and 1b show the XRD patterns of the nanotubes and nanoribbons obtained through a solvothermal route at 180 °C and 160 °C, respectively. Figure 1c is the XRD pattern of the sample obtained under hydrothermal conditions without any surfactant, while Figure 1d and 1e are the spectra of the CATB-assisted and PEG-assisted microspheres, respectively. Despite their morphology difference, the XRD patterns of all the samples present similar profiles and all the diffraction peaks can be indexed to a hexagonal phase of $ZnIn_2S_4$ (ICDD-JCPDS card No. 72-0773, a = 3.85 Å, c = 24.68 Å). No other impurities, such as binary sulfides, oxides, or organic compounds related to reactants, were detected by XRD analysis, indicating the phase purity of the $ZnIn_2S_4$ product. It is noted that the corresponding

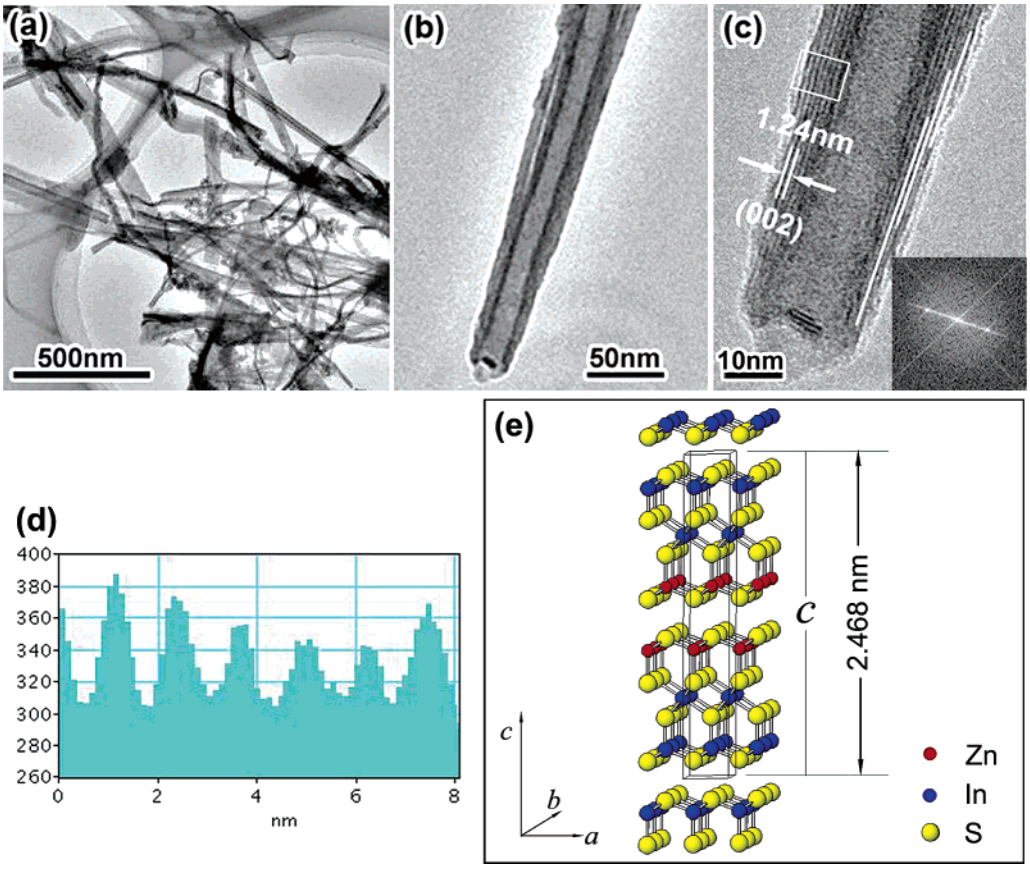

Figure 2. (a, b) TEM micrographs at different magnifications of the $ZnIn_2S_4$ nanotubes prepared by the solvothermal method at 180 °C. (c) HRTEM image of a single nanotube, showing the cone-shaped outer wall and the clear layer fringes; the inset shows the corresponding FFT pattern. (d) Line profile from the area marked with the rectangular frame in (c). (e) The crystal structure of the layered $ZnIn_2S_4$.

intensities of a few diffraction peaks among the products are dissimilar in some cases. For example, the peaks of (108) and (1012) are discernible in all three samples obtained under hydrothermal conditions; however, these peaks are not visible for the as-synthesized nanotubes and nanoribbons. This dissimilarity may be attributed to their differences in morphology and microstructure. Furthermore, the intensity of the (002) peak in the XRD pattern of the nanotube (Figure 1a) is particularly strong, indicating the preferential growth orientation of $ZnIn_2S_4$ nanotubes, which is further analyzed by the HRTEM measurement to be presented later.

Characterization of Nanotubes and Nanoribbons. $ZnIn_2S_4$ nanotubes and nanoribbons were prepared by the pyridine-solvothermal method at different temperatures. The representative TEM image of the $ZnIn_2S_4$ samples obtained at 180 °C is shown in Figure 2a, indicating the formation of nanotubes, which are tens of nanometers in diameter and hundreds of nanometers in length. The 1-D nanotubes were observed throughout the sample, and their proportion is estimated to be greater than 60% from the TEM analysis, demonstrating the high yield of nanotubes through the solvothermal route. A typical individual straight $ZnIn_2S_4$ nanotube is shown in Figure 2b. The inner part of the tube is relatively uniform in size with a diameter of about 17 nm, whereas the outer diameter varies gradually along the axis of the tube. The corresponding HRTEM observation in Figure 2c reveals that the nanotube wall is composed of several layers. The interlayer distance calculated from the line profile (Figure 2d) is 1.24 nm, corresponding to the *d* (002) space of hexagonal $ZnIn_2S_4$. From the lattice fringes marked with white lines on the right sidewall, it can be seen that the upper part of the nanotube possesses one more layer than the lower end, which not only explains the variation of the outer diameter along the tube axis but also implies that the $ZnIn_2S_4$ nanotubes are formed from lamellar structures by a "rolling-up mechanism" to be discussed later in this paper. The Fast Fourier Transform (FFT) pattern (the inset of Figure 2c) displays a bright spot line perpendicular to the lattice fringes in Figure 2c, further confirming that the tube grows along the (002) direction of $ZnIn_2S_4$. Figure 2e shows the crystal structure of the layered $ZnIn_2S_4$, in which the stacking of atoms along the *c*-axis is in a repeated sequence of S−Zn−S−In−S−In−S.[15] The cell parameters of $ZnIn_2S_4$ are $a = b = 3.85$ Å, $c = 24.68$ Å. Therefore, the distance of the neighboring fringes shown in Figure 2c is almost consistent with half of the lattice constant along the *c*-axis of the $ZnIn_2S_4$ structure.

In the solvothermal synthesis of $ZnIn_2S_4$ nanostructures, reaction temperature plays an important role in determining the morphology of the product. When the temperature was lower than 170 °C, $ZnIn_2S_4$ nanoribbons rather than nanotubes were produced. Figure 3 displays the TEM and HRTEM images of the sample prepared at 160 °C. Figure 3a shows the overview image of the obtained nanoribbons. Among these ribbons, some are straight and the others are bent. The width of the ribbons is in the range of 40 to 100 nm, and the length is about several micrometers. The magnified image in Figure 3b shows the ribbon-shaped structure more clearly. Since the nanoribbons are

(15) Donika, F. G.; Radautsan, S. I.; Kiosse, G. A.; Semiletov, S. A.; Donika, T. V.; Mustya, I. G. *Sov. Phys. Crystallogr.* **1971**, *16*, 190.

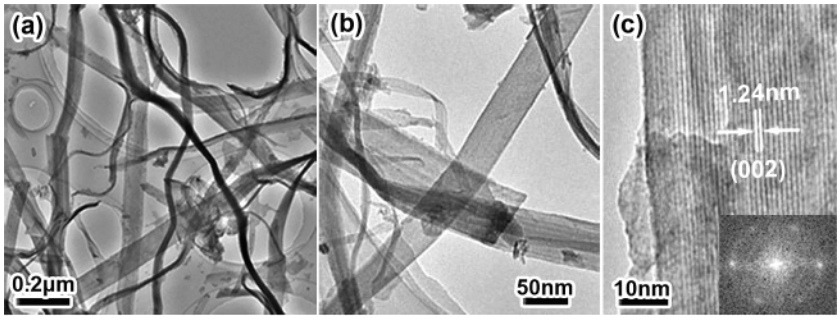

Figure 3. $ZnIn_2S_4$ nanoribbons prepared from the solvothermal synthesis at 160 °C: (a, b) TEM images of the nanoribbons at low and higher magnification, respectively; (c) HRTEM image of a single nanoribbon, clearly revealing its lattice fringes. The inset of (c) shows the corresponding FFT pattern.

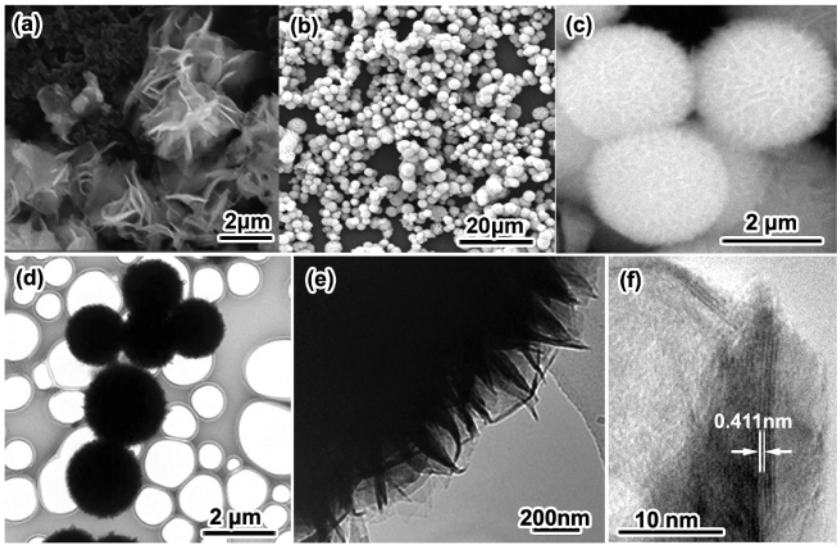

Figure 4. (a) SEM image of the $ZnIn_2S_4$ sample prepared through a hydrothermal route without any surfactant. (b, c) SEM and (d, e) TEM micrographs of the CTAB-assisted $ZnIn_2S_4$ microspheres. (f) HRTEM image of an individual nanowhisker on the surface of a microsphere.

only several nanometers in thickness, they are prone to crinkle or curl under certain conditions such as under high pressure and at high temperature. This is consistent with the demonstrated fact that tubular structure is favored at relatively higher temperatures. The HRTEM image (Figure 3c) indicates the crystalline nature of the nanoribbons, and the separation of lattice fringes is measured as 1.24 nm, identical to that of $ZnIn_2S_4$ nanotubes, revealing that the crystal growth of both nanoribbons and nanotubes undergoes a similar process. Moreover, the FFT pattern (inset of Figure 3c) further substantiates that the $ZnIn_2S_4$ nanoribbon is of a hexagonal phase.

Characterization of Microspheres. It was found that the solvent used in the synthetic system has an important influence on the morphology of $ZnIn_2S_4$. By replacing pyridine with water, the product is composed of irregular sheets (Figure 4a). This growth tendency of lamellar structures might be related to the layered feature of hexagonal $ZnIn_2S_4$. To control the morphology of $ZnIn_2S_4$ under hydrothermal conditions, surfactants such as CTAB and PEG were employed. With the assistance of CTAB, the product is of monodisperse microspheres rather than disordered sheetlike aggregates (Figure 4b), indicating the apparent influence of CTAB on the morphology of $ZnIn_2S_4$. The high-magnification SEM image (Figure 4c) further confirms the uniformity of microspheres, with an average diameter of about 2 μm. Furthermore, all the microspheres maintained their integrity despite vigorous ultrasonic treatment applied to them prior to the TEM measurement, showing the structural robustness of the obtained spheres (Figure 4d). Figure 4e shows a zoomed fraction of the edge of a sphere, revealing that lots of nanowhiskers protrude out of the surface. A representative HRTEM image (Figure 4f) of an individual nanowhisker shows clear lattice fringes. The distance between two neighboring fringes is determined to be about 0.411 nm, which agrees with the d (006) spacing of the hexagonal $ZnIn_2S_4$.

When PEG-6000 was introduced to the hydrothermal reaction system, the morphology of the as-synthesized $ZnIn_2S_4$ product was also mainly of spherelike shapes, as shown in Figure 5a. However, compared to the CTAB-assisted spheres, the PEG-6000 assisted microspheres are not uniform in size, as diamters range from 500 nm to 10 μm. Figure 5b is an enlargement of the square region marked in Figure 5a, and it shows the presence of a typical opening hollow microsphere. To analyze the specific structure of the microspheres, the typical TEM images of the PEG-6000 assisted $ZnIn_2S_4$ samples after ultrasonic dispersion for 20, 40, and 60 min were taken and are shown in Figure 5c, d, and e, respectively. It can be seen that an ultrasonic treatment of 20 min made the $ZnIn_2S_4$ spheres become looser, and a few nanowires are found on the periphery (Figure 5c). With the ultrasonic time prolonged to 40 min, the $ZnIn_2S_4$ spheres are almost entirely disintegrated, and large quantities of nanowires can be observed (Figure 5d). Meanwhile, the undispersed fragments indicated by the arrows coexist with nanowires. After ultrasonic dispersion for 60 min, we can obtain completely dispersive $ZnIn_2S_4$ nanowires (Figure 5e), with a diameter of

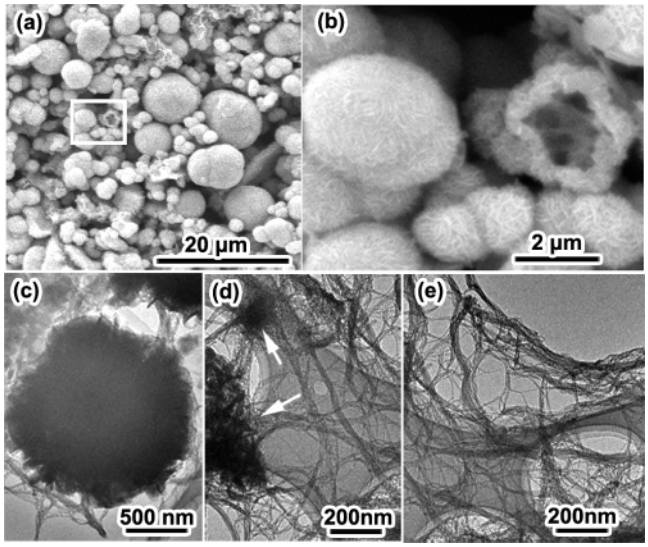

Figure 5. (a) SEM micrograph of the PEG-6000 assisted $ZnIn_2S_4$ microspheres. (b) High-magnification SEM image of the square marked in (a). (c, d, e) TEM images of the PEG-6000 assisted $ZnIn_2S_4$ samples after ultrasonic dispersion for 20, 40, and 60 min, respectively.

about 20−40 nm and a length of several tens of micrometers. Therefore, based on such experimental results, the PEG-6000 assisted $ZnIn_2S_4$ microspheres are essentially composed of $ZnIn_2S_4$ nanowires that entwine like wool coils.

Optical Properties. UV−visible diffuse reflectance spectra (see Supporting Information Figure S1) were measured for the as-prepared $ZnIn_2S_4$ nano- and micromaterials to investigate the possible influence of their shapes and sizes on the optical properties. In a wide wavelength range from UV to visible light, all the samples present a strong absorption with a steep shape on the visible edge. However, their absorption edges are located at different wavelengths: 515 nm for nanowires, 525 nm for nanotubes, 550 nm for nanoribbons, 560 nm for PEG-assisted microspheres, and 570 nm for CTAB-assisted microspheres. The corresponding band gaps of the $ZnIn_2S_4$ samples, calculated from the onset of the absorption edges, are 2.40, 2.38, 2.25, 2.21, and 2.17 eV, respectively. This suggests that the absorption edges blue-shift slightly with the size reduction of $ZnIn_2S_4$. Similar phenomena were observed in other cases such as cadmium selenide and metal nanocrystals.[16,17] Theoretical analysis is still demanded to further understand the correlation between the optical properties and the size/shape of $ZnIn_2S_4$.

The room temperature photoluminescence spectra (shown in Supporting Information Figure S2) of the CTAB-assisted $ZnIn_2S_4$ microspheres present a sharp excitation peak at 573 nm (Figure S2, curve a). This value is in agreement with the band gap of a $ZnIn_2S_4$ microsphere as calculated from the corresponding UV−vis absorption edge. The emission spectrum of the microspheres excited at 573 nm reveals a stable and strong red emission band centered at 784 nm (Figure S2, curve b), comparable to the reported data for $ZnIn_2S_4$ single crystals.[18]

4. Discussions

Phase Formation Mechanism. $ZnIn_2S_4$ can be grown into two distinct polymorphs, either hexagonal or cubic lattices, depending on the synthetic method used.[19] The hexagonal polymorph of $ZnIn_2S_4$ also exhibits different polytypes due to the different stacking fashions of sulfur atoms.[20] In all polytypes of the hexagonal phase, Zn and half of the In atoms are tetrahedrally coordinated by sulfur atoms, whereas the other half are octahedrally coordinated. However, in the case of the cubic phase of $ZnIn_2S_4$, Zn atoms are tetrahedrally coordinated by sulfur atoms, while In atoms are only octahedrally coordinated.

A solution coordination model (SCM) was previously proposed to explain the formation of cubic $ZnIn_2S_4$.[21] According to this model, the coordination of the ions formed in solution serves as a template to retain the same coordination as in the solid. Thus the phase of the solid product is determined by the coordination manner in the solution. The tetrahedral coordinations between the S and the two metal ions (Zn^{2+} and In^{3+}) result in the formation of a cubic phase. On the basis of the above-mentioned SCM model, we propose a formation mechanism of the as-synthesized hexagonal $ZnIn_2S_4$, as illustrated by Figure 6. In solution, In^{3+} and Zn^{2+} can form three different complexes with TAA as the tetrahedral $[In(TAA)_4]^{3+}$ and $[Zn(TAA)_4]^{2+}$ and the octahedral $[In(TAA)_6]^{3+}$. As a result, $In-S_6$, $In-S_4$, and $Zn-S_4$ species are formed under solvothermal or hydrothermal conditions. Meanwhile, these freshly generated metal sulfur species further combine in situ, resulting in a thermodynamically stable hexagonal $ZnIn_2S_4$ phase in which the coordination of In^{3+} ions is present in both the octahedral and the tetrahedral forms. The above-proposed mechanism was further indirectly supported by the XRD analysis (Supporting Information Figure S3) of the solid product obtained after reacting for 10 min under hydrothermal conditions. We have found that, even in such a short reaction time, the hexagonal-phase of $ZnIn_2S_4$ is the only solid product, and there is no evidence of the formation of a cubic phase or binary sulfides such as ZnS and In_2S_3.

Formation of 1-D Nanostructures. 1-D ternary chalcogenide nanostructures have rarely been investigated until now, so the formation mechanism of $ZnIn_2S_4$ nanotubes and nanoribbons is of particular interest. In the present synthesis, a solution-based method is developed for the direct growth of 1-D ternary chalcogenide nanostructures without any catalysts or templates. The experimental results suggest that the formation of 1-D $ZnIn_2S_4$ nanostructures involves a nucleation step and a self-growth step, as described in Figure 7. First, $ZnIn_2S_4$ nuclei are spontaneously formed through the reaction among $ZnSO_4 \cdot 7H_2O$, $InCl_3 \cdot 4H_2O$, and TAA. Then, these newly produced nuclei self-assemble in situ, and driven by the anisotropy growth tendence of hexagonal crystal structure, they grow anisotropically into $ZnIn_2S_4$ lamellar mesostructures. In the next stage, the freshly generated $ZnIn_2S_4$ layered intermediates proceed in two ways: (a) under appropriate conditions, they may roll up into tubes (Figure 2), analogous to the natural phenomena of a piece of wet paper curling into scrolls during its drying process;[22] (b) they may grow directly along the (002) direction to form nanoribbons (Figure 3).

(16) Peng, X.; Manna, L.; Yang, W.; Wickham, J.; Scher, E.; Kadavanich, A.; Alivisatos, A. P. *Nature* **2000**, *404*, 59.
(17) Hao, E.; Li, S.; Bailey, R. C.; Zou, S.; Schatz, G. C.; Hupp, J. T. *J. Phys. Chem. B* **2004**, *108*, 1224.
(18) Shionaoya, S.; Tamoto, Y. *J. Phys. Soc. Jpn.* **1964**, *19*, 1142.
(19) Lopez-Revera, S. A.; Mora, A. J.; Najarro, D. A.; Rivera, A. V.; Godoy, R. A. *Semicond. Sci. Technol.* **2001**, *16*, 367.
(20) Tinoco, T.; Polian, A.; Itié, J. P.; López, S. A. *Phys. Status Solidi B* **1999**, *211*, 385.
(21) Sriram, M. A.; Mcmichael, P. H.; Waghray, A.; Kumta, P. N. *J. Mater. Sci.* **1998**, *33*, 4333.

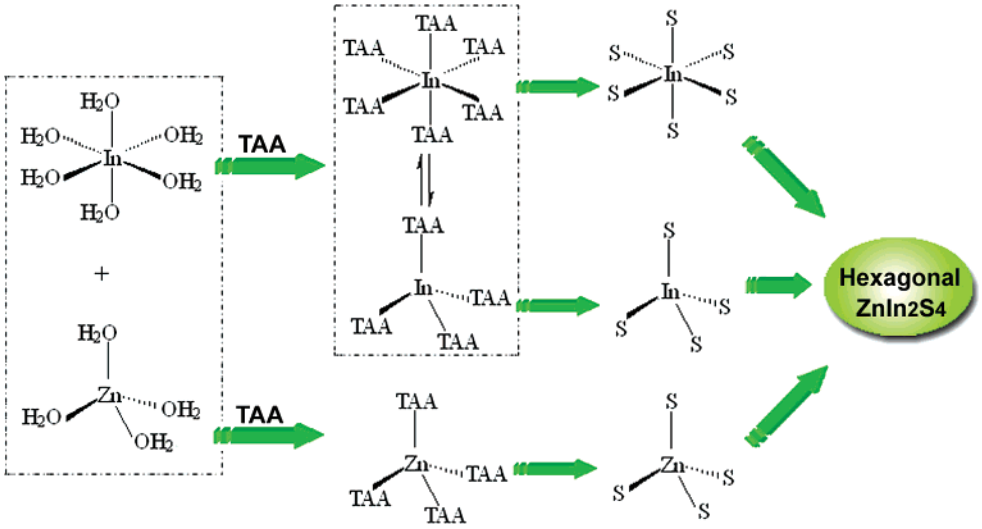

Figure 6. Schematic illustration showing the formation of hexagonal $ZnIn_2S_4$. For clarity, the charges for the complexes are omitted in the figure.

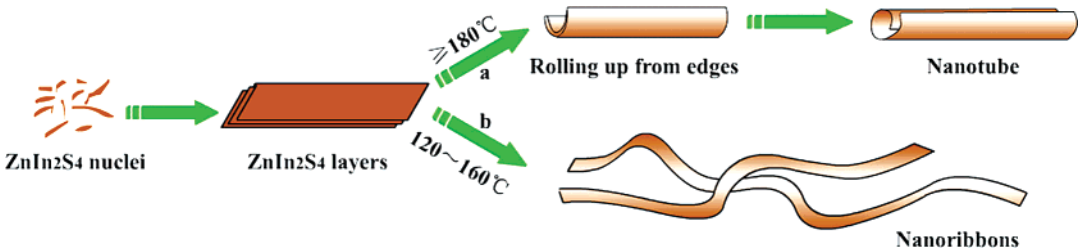

Figure 7. Schematic depiction of the proposed growth mechanism for $ZnIn_2S_4$ nanotubes (a) and nanoribbons (b).

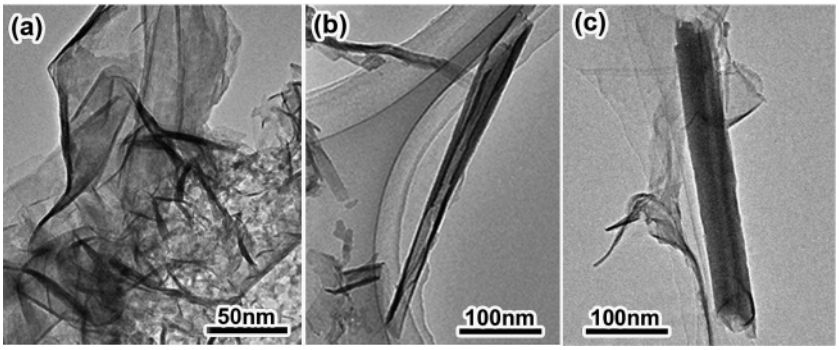

Figure 8. TEM images of the $ZnIn_2S_4$ samples obtained at 180 °C after solvothermal reaction for 2 h (a), 8 h (b), and 12 h (c), respectively, confirming the rolling growth process of a $ZnIn_2S_4$ nanotube from lamellar structures.

Controlled experiments and extensive TEM observations were carried out to understand the above-proposed mechanism. We have found that the temperature and the duration of the solvothermal treatment were crucial to the final morphology. When the reaction temperature was between 160 °C and 120 °C, only nanoribbons were formed (Figure 3 and Supporting Information Figure S4). At an elevated temperature of 180 °C, the $ZnIn_2S_4$ lamellar structures started to curl from the edges of the layers (Figure 8a) after aging the reaction system for 2 h. With the prolonged heating time, the rolling process continued (Figure 8b and c) and a uniformly shaped $ZnIn_2S_4$ nanotube was finally achieved after sufficient duration of the solvothermal treatment (Figure 2). Therefore, a high temperature and long heating time may favor the curling of layered sheets, leading to the formation of tubular structures, whereas lower synthesis temperatures always result in a ribbonlike product. This result suggests that, during the rolling process of lamellar intermediates, enough energy should be provided to overcome the strain energy barrier, as has been demonstrated in previous literature.[23] Moreover, HRTEM images and the corresponding FFT patterns (Figures 2c and 3c) reveal the close relationship between $ZnIn_2S_4$ nanotubes and nanoribbons due to their crystalline similarity. These experimental results and analyses support the proposed growth mechanism of $ZnIn_2S_4$ one-dimensional nanostructures that is illustrated in Figure 7.

The above results indicate that $ZnIn_2S_4$ nanotubes and nanoribbons can be selectively synthesized merely by controlling the temperature and the duration of the solvothermal reaction. It should be noted that pyridine plays a significant role in the selective synthesis. Parallel experiments were carried out by substituting pyridine with other solvents such as water, alcohol,

(22) Li, Y. D.; Li, X. L.; He, R. R.; Zhu, J.; Deng, Z. X. *J. Am. Chem. Soc.* **2002**, *124*, 1411.

(23) Tenne, R. *Angew. Chem., Int. Ed.* **2003**, *42*, 5124.

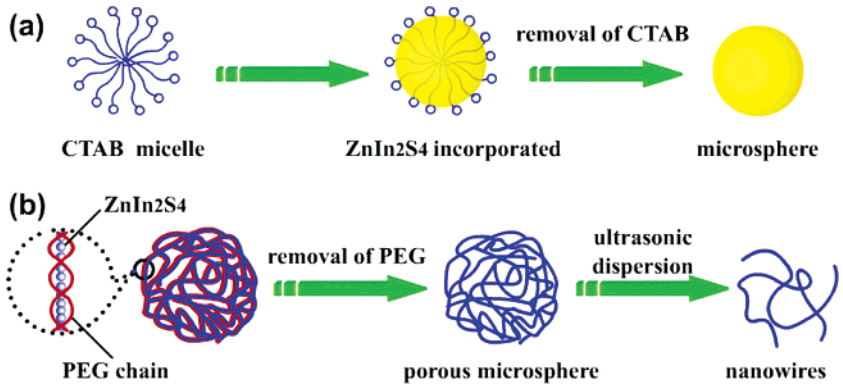

Figure 9. Schematic illustration of the possible growth mechanism of $ZnIn_2S_4$ microsphere and nanowires obtained in the presence of (a) CTAB and (b) PEG-6000.

tetrahydrofuran, and acetonitrile; however, neither nanotubes nor nanoribbons were observed under similar conditions. This may be attributed to the differences of these solvents in alkalinity, coordination ability, viscosity, surface tension, or dipole moment, which are all important factors in influencing the shape/size of the product in solvothermal synthesis.[2c,24]

Formation of Microspheres. Organic surfactants can act as structure-directing agents or "soft templates" and are widely used to prepare nanostructured materials with peculiar morphologies.[25] For example, with the aid of CTAB or PEG, a variety of inorganic nanostructures with novel morphologies have been constructed.[26,27] In the present work, the addition of surfactants leads to a distinct difference in the morphologies of the products. Therefore, it is reasonable to speculate that both CTAB and PEG play important roles in controlling the morphology of $ZnIn_2S_4$. CTAB-assisted microspheres are robust enough to withstand vigorous ultrasonic treatment (Figure 4d), whereas the PEG-assisted hollow microspheres (Figure 5b) are unconsolidated and can be dispersed to $ZnIn_2S_4$ nanowires (Figure 5c−e) when subjected to ultrasonic treatment. Based on the SEM and TEM observations, we propose a morphology-controlled mechanism as demonstrated in Figure 9. Due to their structural difference, CTAB and PEG exhibit different behaviors in an aqueous solution. CTAB self-organizes into spherical micelles (Figure 9a) because of its polar hydrophilic heads (N terminal, blue circles) and hydrophobic alkyl chains. Inorganic species such as Zn^{2+}, In^{3+}, and TAA enter into and incorporate these spherical CTAB micelles. The subsequent nucleation and crystal growth of $ZnIn_2S_4$ occur in the micelles, leading to the formation of uniform and robust $ZnIn_2S_4$ microspheres after the removal of CTAB.

Unlike CTAB, the nonionic surfactant PEG-6000 can form long chains in water. In addition, a large amount of active oxygen atoms exist in PEG molecular chains, resulting in strong interactions between PEG chains and metal ions. The nucleation and crystal growth of $ZnIn_2S_4$ are confined within the chains (Figure 9b); thus the anisotropy crystal growth leads to the formation of nanowires, which possess large aspect ratios. On the other hand, since the PEG long chains are flexible enough to interweave, the nanowires thereby tend to form incompact spherical aggregates with a cavity-network structure (Figure 5b) due to the hydrogen-bonding effect. After removing PEG-6000, the hollow spheres that essentially consist of nanowires are obtained. Because PEG chains may intertwist in different modes, the shape of the resultant spheres is not uniform and the diameters are uneven. When the product was ultrasonically dispersed for an extended period of time (for example, 1 h), $ZnIn_2S_4$ nanowires became untwisted and were released completely from the fibrous spheres (Figure 5e).

Since $ZnIn_2S_4$ materials can be synthesized with controlled shapes through the solution-based route, we further extended such a solution-based method to the synthesis of other ternary chalcogenide compounds. $CuInS_2$ and $CuInSe_2$ nano- and microscaled materials with different surface morphologies (see Supporting Information Figure S5) including spheres, platelets, rods, and fishbonelike shapes were obtained by using similar hydrothermal and solvothermal methods.

Recently, Nanu et al. reported the preparation of three-dimensional (3-D) solar cells that were composed of TiO_2/$CuInS_2$ nanocomposites, with a remarkable energy conversion efficiency of 5%.[8a] They suggested that the improved performance of the 3-D nanocomposite solar cells could be attributed to the enhanced interface recombination of electron−hole pairs in the light-absorbing nanomaterials. Therefore, our further work will focus on application of the as-synthesized ternary chalcogenide microstructures in solar cells.

5. Conclusions

Ternary chalcogenide $ZnIn_2S_4$ 1-D nanostructures and microspheres of hexagonal crystal phase have been successfully synthesized through a facile solution-chemistry route. By controlling the reaction conditions, $ZnIn_2S_4$ nanotubes, nanoribbons, nanowires, and microspheres can be selectively prepared. These nano- and microstructures exhibit strong absorption in a wide wavelength range from visible to UV light, and the obtained microspheres show intense excitation and emission luminescence at room temperature. A phase formation mechanism and morphology-controlled process have been proposed and discussed on the basis of experimental data. Furthermore, the solution chemistry route is found to be applicable to the synthesis of $CuInS_2$ and $CuInSe_2$ microspheres with different surface morphologies. The present work would give some

(24) Walton, R. I. *Chem. Soc. Rev.* **2002**, *31*, 230.
(25) (a) Schüth, F. *Angew. Chem., Int. Ed.* **2003**, *42*, 3604. (b) Bommel, K. J. C.; Friggeri, A.; Shinkai, S. *Angew. Chem., Int. Ed.* **2003**, *42*, 980.
(26) (a) Wang, W.; Poudel, B.; Yang, J.; Wang, D. Z.; Ren, Z. F. *J. Am. Chem. Soc.* **2005**, *127*, 13792. (b) Korlann, S. D.; Riley, A. E.; Kirsch, B. L.; Mun, B. S.; Tolbert, S. H. *J. Am. Chem. Soc.* **2005**, *127*, 12516.
(27) (a) Chen, J.; Burger, C.; Krishnan, C. V.; Chu, B. *J. Am. Chem. Soc.* **2005**, *127*, 14140. (b) Cheng, F. Y.; Chen, J.; Gou, X. L.; Shen, P. W. *Adv. Mater.* **2005**, *17*, 2753.

elicitations to the controllable synthesis of ternary chalcogenide nano- and micromaterials.

Acknowledgment. This work was supported by the Outstanding Young Scientific Foundation of NSFC (20325102) and National Key Basic Research Program (2005CB623607).

Supporting Information Available: UV−vis absorption spectra and photoluminescence spectra of the $ZnIn_2S_4$ samples with different morphologies; TEM images of $ZnIn_2S_4$ nanoribbons prepared at different temperatures; XRD pattern of the $ZnIn_2S_4$ solid sample obtained after hydrothermal reaction for 10 min; SEM images of the as-synthesized $CuInS_2$ and $CuInSe_2$ samples. This material is available free of charge via the Internet at http://pubs.acs.org.

JA0580845